Collisional scattering of strongly interacting *D*-band Feshbach molecules in optical lattices

Fansu Wei,[1] Chi-Kin Lai,[1] Yuying Chen,[2] Zhengxi Zhang,[1] Yun Liang,[1] Hongmian Shui,[1,3] Chen Li,[4,*] and Xiaoji Zhou[1,3,†]

[1]*State Key Laboratory of Advanced Optical Communication Systems and Networks, School of Electronics, Peking University, Beijing 100871, China*

[2]*School of Physics and Electronics Engineering, Shanxi University, Taiyuan 030006, China*

[3]*Institute of Carbon-based Thin Film Electronics, Peking University, Shanxi, Taiyuan 030012, China*

[4]*Vienna Center for Quantum Science and Technology, Atominstitut, TU Wien, Stadionallee 2, 1020 Vienna, Austria*

(Received 10 December 2024; accepted 25 March 2025; published 9 April 2025)

The excited bands in optical lattices manifest an important tool for studying quantum simulation and many-body physics, making it crucial to measure high-band scattering dynamics under strong interactions. This work investigates both experimentally and theoretically the collisional scattering of $^6Li_2$ molecular Bose-Einstein condensate in the *D* band of a one-dimensional optical lattice, with interaction strength directly tunable via magnetic Feshbach resonance. We find a clear dependence of the *D*-band lifetimes on the interaction strength within the strongly interacting regime, which arises from the fact that the scattering cross section is proportional to the square of the scattering length. The maximum lifetime versus lattice depth is measured to reveal the effects of interactions. We also investigate the scattering channels of *D*-band molecules under different interaction levels and develop a reliable two-body scattering rate equation. This work provides insight into the interplay between interaction and the collisional scattering of high-band bosons in optical lattices, paving the way for research into strong correlation effects in high-band lattice systems.

DOI: 10.1103/PhysRevResearch.7.023030

I. INTRODUCTION

Quantum gases confined in optical lattices have emerged as a versatile platform for exploring fundamental physics, particularly in many-body systems, due to their high controllability and robustness [1]. These systems allow for the simulation of complex phenomena, such as phase transitions [2–5], quantum magnetism [6,7], and strongly correlated systems [8–10]. An intriguing aspect of these systems is the study of excited bands, which provide insights into the production of novel quantum phases [11–16] and the dynamics of external states [17–19].

Collisional scattering is one of the most fundamental interaction processes in many-body systems. Research has focused on low-energy collisions within various systems, including atomic [20–25], ionic [26,27], and electronic systems [28–30]. This process is particularly significant in the context of quantum gases, where the system's lifetime is strictly inversely proportional to the two-body collision rate in most cases. The scattering cross section, which characterizes the two-body collision rate, has been extensively investigated both experimentally and theoretically in one-, two-, and mixed-dimensional optical lattices [31–36], such as the scattering model for atoms in the *P* band of a one-dimensional (1D) lattice [36], the measurement of the collision rate for atoms in the *D* band of a 2D triangular lattice [37,38] and the observation of scattering halos [39,40], etc.

In most cases, quantum simulation based on the excited bands [41–44] is significantly influenced by the collisional scattering regardless of the interaction levels. However, previous works have only studied the impact of parameters such as lattice depth and gas temperature on collision scattering in the weakly interacting regime. Currently, due to the difficulty of accurately tuning interactions in condensed excited-band systems in optical lattices, there is no reliable experimental evidence to verify the correspondence between interactions and excited band collision scattering rates within the strongly interacting regime.

In this study, we explore both experimentally and theoretically the collisional scattering and lifetimes of $^6Li_2$ molecular Bose-Einstein condensates (mBEC) in the *D* band of a 1D optical lattice. Our main focus is on the impact of interparticle interactions on scattering rates and processes, with the interaction strength precisely adjustable via magnetic Feshbach resonance. We present measurements of the lifetimes of *D*-band molecules under various interparticle interactions and lattice depths, revealing the squared relationship between *D*-band scattering rates and scattering lengths within a certain strongly interacting regime. The *D*-band lifetimes are meticulously measured as a function of lattice depth, and the discrepancies between experimental results and theoretical predictions are analyzed and discussed. Furthermore, we examine the *D*-band scattering processes in both the strongly interacting $^6Li_2$ system and weakly interacting ^{87}Rb system, with the latter demonstrating strong agreement with the rate

*Contact author: chen.li@tuwien.ac.at
†Contact author: xjzhou@pku.edu.cn

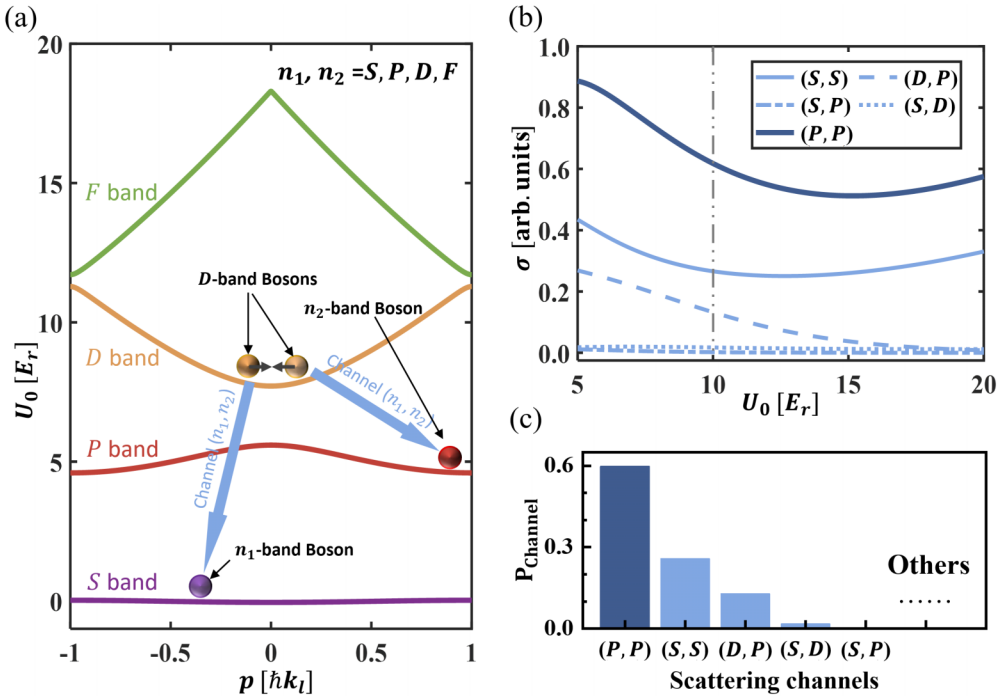

FIG. 1. (a) Band structure of a 1D lattice and two-body scattering processes in the D band. Two D-band bosons collide and each transitions into separate bands with lower total energy. (b) Relative scattering cross sections are given by the theoretical model. The dark blue solid line marks the relative scattering cross sections of (D, D) to (P, P), and the shallow blue solid line, dashed line, dotted line, and dash-dotted line mark (D, D) to (S, S), (D, P), (S, D), and (S, P), respectively, under different lattice depths. (c) The relative proportion of channels with the lattice depth $U_0 = 10E_r$. The proportions of other channels are close to zero and can be considered negligible. Note that these scattering cross sections are calculated in weak-interacting conditions.

equation model developed in this study. We discuss the discrepancies between the two in depth and qualitatively analyze the interactions' role.

This paper is organized as follows. In Sec. II, the theoretical model for the collisional scattering of D-band particles in a 1D optical lattice is described. Our experimental procedure, including the shortcut loading into the D band and lifetime measurement, is shown in Sec. III. In Sec. IV, we present the experimental results of D-band lifetimes with varying interaction strengths and lattice depths. The experimental results of scattering channels and the rate equation model are described in Sec. V with a discussion. Finally, we give the conclusion in Sec. VI.

II. THEORETICAL MODEL OF EXCITED-BAND SCATTERING

For ultracold bosons in the excited band of optical lattices, two-body collisions induced by s-wave scattering serve as the primary decay mechanism. In these collisions, two bosons in excited-energy bands collide and each scatters into the energy states with lower total energy. Here we introduce the two-body scattering model in a 1D optical lattice, with the Hamiltonian given by

$$\hat{H} = -\frac{\hbar^2}{m}\left(\frac{\partial^2}{\partial y^2} + \frac{\partial^2}{\partial z^2}\right) + \sum_{i=1,2} -\frac{\hbar^2}{2m}\frac{\partial^2}{\partial x_i^2} + U_0 \cos^2\left(\frac{\pi x}{L}\right) + \frac{4\pi\hbar^2 a_s}{m}\delta(\mathbf{r})\frac{\partial}{\partial r}(r\cdot), \tag{1}$$

where $\mathbf{r}_1$, $\mathbf{r}_2$ are the coordinates of two bosons, with $\mathbf{r} = \mathbf{r}_2 - \mathbf{r}_1$; U_0 is the lattice depth; L is the lattice constant; and a_s is the s-wave scattering length. As illustrated in Fig. 1(a), two bosons initially in D band scatter into the final bands (n_1, n_2) through the first-order scattering process, which depends on the overlapping integral defined as [35]:

$$\Gamma^{D,D}_{n_1,n_2}(q_1', q_2'; q_1, q_2) = \int_0^L \mathrm{d}x\, u^*_{n_1,q_1}(x) u^*_{n_2,q_2}(x) u_{D,q_1'}(x) u_{D,q_2'}(x), \tag{2}$$

where u_{n_i,q_i} is the periodic Bloch function for bosons in energy band n_i with quasimomentum q_i. Moreover, the scattering cross section is given by:

$$\sigma(D, D; n_1, n_2)v = \frac{8\pi a_s^2 L^2}{m}\int \mathrm{d}q\mathrm{d}q_1\mathrm{d}q_2\ \Xi(q_1, q_2)\theta\left(E_{D,q_1} + E_{D,q_2} - E_{n_1,(q_1+q_2)/2+q} - E_{n_2,(q_1+q_2)/2-q}\right) \times \left|\Gamma^{D,D}_{n_1,n_2}(q_1, q_2; (q_1+q_2)/2+q, (q_1+q_2)/2-q)\right|^2, \tag{3}$$

where v is the relative velocity of the two bosons, $\Xi(q_1, q_2)$ is the quasimomentum distribution of the two bosons, and $\theta(x)$ is the Heaviside step function defined as $\theta(x) = 1$ when $x \geqslant 0$ and $\theta(x) = 0$ when $x < 0$. E_{n_i,q_i} is the single-atom energy. This scattering cross section quantifies the strength of the interband or intraband scattering process, namely the scattering channel.

For two bosons in D band, the possible final bands after scattering include $(n_1, n_2) = (S, S)$, (P, P), (S, P), (P, D), and (S, D). In the weakly interacting regime, where the momentum broadening effect is negligible, the scattering cross sections can be calculated by approximating the two-body quasimomentum distribution in the D band as $\Xi(q_1, q_2) \approx \delta(q_1)\delta(q_2)$ in Eq. (3). Applying this approximation, the relative scattering cross sections in the weakly interacting system with varying lattice depths are presented in Fig. 1(b). It shows that across all lattice depths, the scattering cross section for $(D, D) \rightarrow (P, P)$ (the dark blue solid line) is the largest, followed by $(D, D) \rightarrow (S, S)$ (the shallow blue solid line). Specifically, we demonstrate the relative cross section when $U_0 = 10E_r$ in Fig. 1(c), which shows the dominant scattering channel is $(D, D) \rightarrow (P, P)$ due to the large overlap between the wave functions [38]. It is noteworthy that D-band bosons undergoing the first scattering event may further experience secondary scattering, thus making the results of D-band scattering different from the theoretical predictions above.

Given the s-wave scattering length a_s, the scattering rate of the D-band bosons, $K(D, D)$, can be calculated by summing over the cross sections of all possible scattering channels:

$$K(D, D) = n_D \sum_{n_1,n_2} \sigma(D, D; n_1, n_2)v = n_D R(U_0) a_s^2, \qquad (4)$$

where $R(U_0)$ is a function of U_0 determined by the scattering cross sections and n_D is the density of D-band bosons held in the optical lattices. Therefore, the lifetime of D-band bosons, τ, can be estimated by the initial scattering rate $K^i(d, d)$:

$$\tau \propto \frac{1}{K^i(D, D)} = \frac{1}{n_D^i R(U_0) a_s^2}, \qquad (5)$$

where n_D^i is the initial density of bosons in the D band after loading.

In this manner, we theoretically predict the factors influencing the scattering rates of D-band bosons and identify the dominant scattering channel. Experimental validation of these predictions requires low particle temperatures, rapid preparation of D-band occupation (relative to the timescale of scattering lifetimes), and the capability to directly control scattering lengths.

III. EXPERIMENTAL DEMONSTRATION

To study the above collisional scattering phenomena, our experiments are performed with BECs of ^{6}Li Feshbach molecules [45], with each molecule constituted by two lithium atoms in the lowest hyperfine states $|F = 1/2, m_F = 1/2\rangle$ ($|1\rangle$) and $|F = 1/2, m_F = -1/2\rangle$ ($|2\rangle$). The intermolecule interaction strength can be set over a range by tuning the s-wave scattering length a_{12} between atoms in states $|1\rangle$ and $|2\rangle$ via the Feshbach resonance [46] and the s-wave scattering length between molecules is given by $a_s = 0.6a_{12}$ [47].

Figure 2(a) shows the schematic of the experimental setup (full details provided in Ref. [43]). The mBECs of about 20 000 molecules are confined in the crossed optical dipole traps formed by a pair of far-red-detuned lasers in a vertical plane with a 30° to each other. A pair of hollow electric coils produce the Feshbach Resonance magnetic field. The trapping frequencies are $(\omega_x, \omega_y, \omega_z) = 2\pi \times (39.5, 187.8, 195.0)$ Hz, where the x axis refers to the horizontal direction where the plane trapping beams are located, the y axis the other horizontal direction, and the z axis the vertical direction. The one-dimensional optical lattice is formed by two counterpropagating beams of $\lambda = 1064$-nm lasers resulting in a lattice constant $L = \lambda/2 = 532$ nm, with lattice potential $U(x) = U_0 \cos^2(\pi x/L)$ in the horizontal direction, where U_0 is the lattice depth. The characteristic lattice energy is $E_r = \hbar^2 {k_l}^2/2m$, where $k_l = \pi/L$ and m is the mass of a ^{6}Li$_2$ molecule.

The experimental time sequence is presented in Fig. 2(b). After evaporative cooling, the degenerate gas is prepared at a temperature of $T/T_F \simeq 0.1$. The Feshbach magnetic field is then adiabatically (300 G/s) ramped to the target value and kept for an additional duration to stabilize. Then a nonadiabatic shortcut method is utilized to load particles from the harmonic trap into the D-band Γ point ($q = 0$) of the lattice. For different lattice depths, which are calibrated by Kaptiza-Dirac (KD) scattering [48], a distinctive sequence of optical pulses with intervals is optimized to reach the target state with high fidelity [44,49]. For instance, a two-pulse sequence $(t_1^{\text{on}}, t_1^{\text{off}}, t_2^{\text{on}}, t_2^{\text{off}}) = (2.9, 6.0, 8.3, 5.4)$ μs is used for the lattice depth $U_0 = 10E_r$ with the theoretical fidelity above 99.5% in the noninteracting limit. This shortcut method can be applied to different lattice depths and interactions while maintaining high fidelity (see Appendix A for details). After the loading process, the D-band mBECs stay in the lattice for a period of evolution time t_{evo}. Then we apply the band mapping method [50] to read out band distribution by ramping down the lattice in the form of $e^{-t_{\text{map}}/\tau}$, where $t_{\text{map}} = 100$ μs and $\tau = 50$ μs. This mapping process projects particles in different bands into the corresponding Brillouin zone (BZ). Thus, molecules at the D-band Γ point are mapped to the boundary between the second and third BZs at $p = \pm 2\hbar k_l$. Finally, the optical dipole traps and the optical lattices are both turned off, and particles in different states expand during a TOF process, which is detected via standard absorption imaging.

A typical distribution of D-band mBECs is shown in Fig. 2(c). This distribution is integrated along the y axis to obtain a one-dimensional density distribution function. Here, we use a bimodal fitting method to obtain the number of molecules in the D band, which is marked by the yellow dashed line in the bottom panel of Fig. 2(c). The function can be expressed as follows:

$$f(p) = A_0 e^{-\frac{(p-p_0)^2}{2w_0^2}} + \sum_{i=1}^{5} A_i \left(1 - \frac{(p - p_i)^2}{w_i^2}\right)^2. \qquad (6)$$

The first term represents the scattering halo, while the second term represents condensed particles at $p = 0$ (S band), $\pm\hbar k_l$ (P band), and $\pm 2\hbar k_l$ (D band). Here A_i are the amplitudes and w_i are their widths. By integrating the corresponding terms,

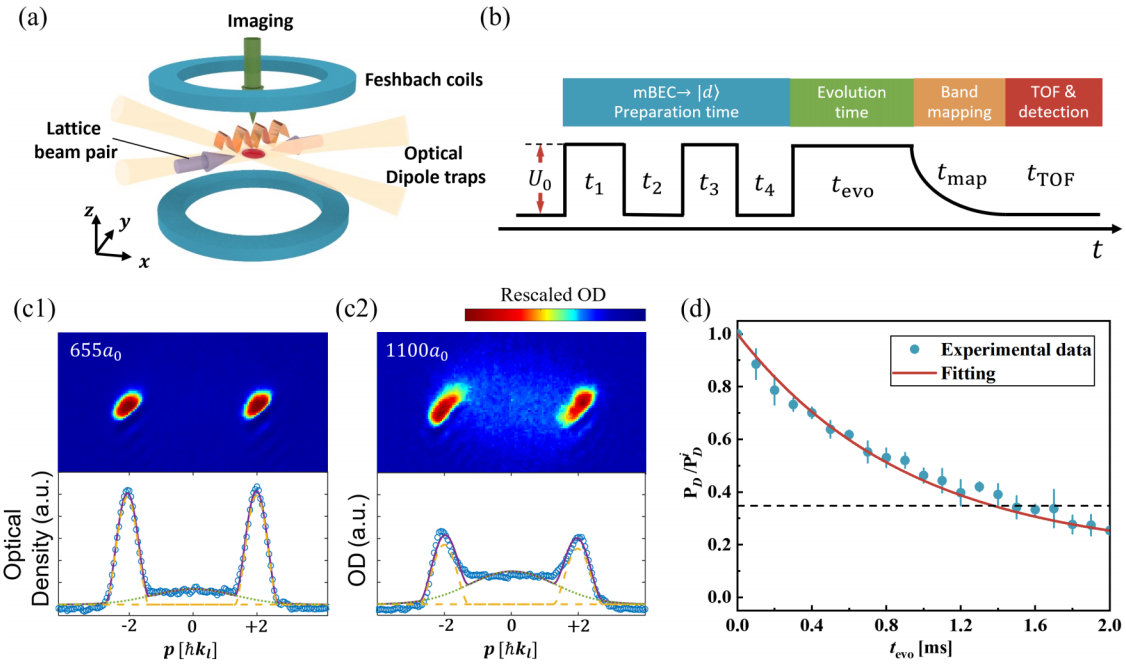

FIG. 2. (a) Schematic of the experimental system. Feshbach mBECs are trapped in a pair of crossover dipole traps. The blue circles in the x-y plane represent the Feshbach magnetic coils and the yellow Gaussian beams along the x axis mark the crossed optical dipole trap. The two purple arrows in the x-y plane denote the counterpropagating lattice beams. The green arrow shows the imaging direction, which is perpendicular to the x-y plane. (b) A typical experimental sequence of the lattice light. After preparing steady mBEC with varying interaction strengths, the lattice sequence will be initiated. The pulses applied before the evolution time $t_{\rm evo}$ are shortcut pulses designed to load mBEC into the D band with lattice depth U_0. The lattice beam intensity decreases to zero adiabatically in time $t_{\rm map}$ to give a band mapping after $t_{\rm evo}$. $t_{\rm TOF}$ represents the time of flight following the complete switch-off of the lattice and trapping potential, after which imaging detection is performed. Experimental stages are shown above. (c) Top: Images taken with $U_0 = 10E_r$, $t_{\rm evo} = 100$ μs, $t_{\rm map} = 100$ μs, and $t_{\rm TOF} = 2$ ms at different interaction strength and (bottom) the corresponding fitting result. (c1) $a_s = 655a_0$. (c2) $a_s = 1100a_0$. (d) Measurement of molecular lifetime in the D band ($U_0 = 10E_r$, $a_s = 655a_0$). The D-band proportion P_D is normalized to $P_D^i \simeq 0.7$, and the error bar shows the standard error of five measurements. The position of $P_D/P_D^i = 1/e$ is marked by the gray dashed line.

we determine the number of particles in the D band (N_D) and the total particle number (N). The results for intermolecule scattering length with $a_s = 655a_0$ [Fig. 2(c1)] and $1100a_0$ [Fig. 2(c2)] are displayed, where a_0 donates the Bohr radius (0.0529 nm). We observe that the larger interactions result in a more prominent scattering halo, which has been investigated in our work [51]. Halo formation primarily stems from collisions during TOF expansion, with a secondary contribution from collisions during the lattice pulse.

Here we define the strongly and weakly interacting regimes based on experiments. In the strongly interacting regime, where $a_s > 500a_0$, there are additional effects beyond the excited-band scattering process, such as coherence loss and more pronounced halos during TOF expansion, whereas in the weakly interacting regime, for $a_s < 100a_0$, the halo and coherence loss are negligible. Despite these additional effects in the strongly interacting regime, the fitting process ensures that our measurements of the D-band proportion remain solid.

The proportion of remaining condensed molecules in the D band over time can be obtained by changing the evolution time $t_{\rm evo}$ in the lattices. As shown in Fig. 2(d), for $a_s = 655a_0$ and $U_0 = 10E_r$ (the laser power ≈250 mW), $P_D = N_D/N$ normalized to the initial proportion $P_D^i = 0.7$ as a function of varied $\tau_{\rm evo}$ is shown by the blue dots, with $\tau_{\rm evo}$ changed every 0.1 ms up to 2 ms. It is fitted by a red solid line to calculate the molecular D-band lifetime with $P_D/P_D^i = 1/e$, and we get the D-band lifetime $\tau = (1.393 \pm 0.071)$ ms in this situation. In this way, we can measure the lifetimes and scattering rates of D-band molecules under different interactions and lattice depths.

IV. INFLUENCE OF INTERACTIONS ON EXCITED-BAND LIFETIMES

According to Eq. (5), D-band lifetime is primarily influenced by three factors: the s-wave scattering length a_s, the initial particle number density n_D^i, and $R(U_0)$, which is determined by the scattering cross section as a function of U_0. The first two factors are directly related to interactions, while U_0 can also influence interactions in optical lattices to some extent. Therefore, in this section, we investigate how the D-band lifetime is affected by the interactions originating from the interplay between a_s and U_0, and the resulting influence as reflected through its trend.

A. The relationship between scattering length and D-band lifetime under varying lattice depths

To explore the relationship between the D-band lifetime and the s-wave scattering length, we measure lifetimes across different lattice depths with varying interaction strengths while maintaining the particle number density nearly constant

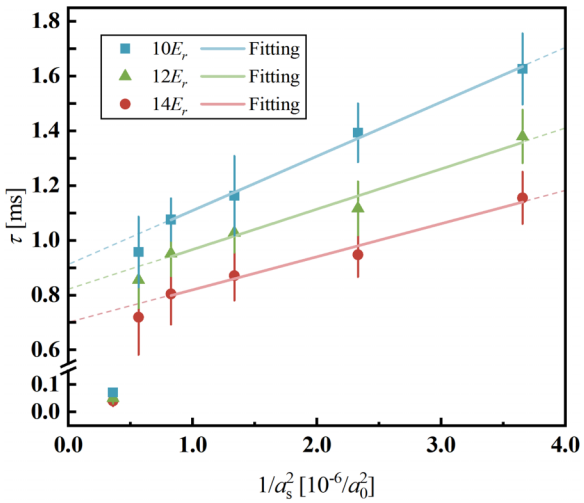

FIG. 3. D-band lifetimes under different interaction strengths ($n_D = 1.0\times10^{18}$ m^{-3}). The blue squares, green triangles, and red circles indicate the results of $U_0 = 10E_r$, $12E_r$, and $14E_r$. The corresponding lines are linear fitting of the four data points with the largest $1/a_s^2$.

($n_D = 1.0\times10^{18}$ m^{-3}) by adiabatically tuning optical dipole traps. The experimental results are presented in the form of $\tau - 1/a_s^2$ to better assess the relationship, in Fig. 3. As an example with $U_0 = 10E_r$, we measure the D-band lifetime for $a_s = 1600a_0$, $1330a_0$, $1100a_0$, $865a_0$, $655a_0$, and $523a_0$, which correspond to the six blue squares from left to right in Fig. 3, respectively. The error bars represent the fitting uncertainty of the lifetimes. Visually, for a given lattice depth, a degree of linearity is observed for the five data points corresponding to the smallest s-wave scattering lengths (i.e., the five largest $1/a_s^2$). But for the largest scattering length ($a_s = 1600a_0$), the lifetimes decrease sharply to less than 100 μs. Linear fits are attempted for both the five and four largest $1/a_s^2$. The fit to the four exhibits superior linearity, achieving R-squared (R^2) values greater than 0.99 across all lattice depths (indicated by the solid lines in Fig. 3). However, the remaining two data points ($a_s = 1600a_0$, $1330a_0$) deviate significantly from the linear relationship, falling below the fitted line.

From the experimental results, we find that the linear relationship between τ and $1/a_s^2$ holds within a certain range, indicating that the scattering rate of the D band is proportional to the square of the scattering length. However, for stronger interactions ($a_s > 1330a_0$), the experimental data do not yield reliable lifetime fittings due to the drastic decay in D-band occupation and influential scattering halos. It suggests that when $a_s \to +\infty$, τ gradually deviates from linearity and converges to zero, marking the failure of excited-band scattering theory. Meanwhile, in the noninteracting regime, the lifetime improves but does not approach infinity due to the nonuniformity of the external harmonic trap and collisions with the background gas.

To summarize, in a certain strongly interacting regime where the scattering length does not diverge, the D-band scattering rate is proportional to a_s^2 and can be supported by our experiments. This relation can be generalized to other excited energy bands with necessary corrections. The scattering behavior in the vicinity of the crossover between interaction regimes presents a promising direction for future experimental and theoretical investigation.

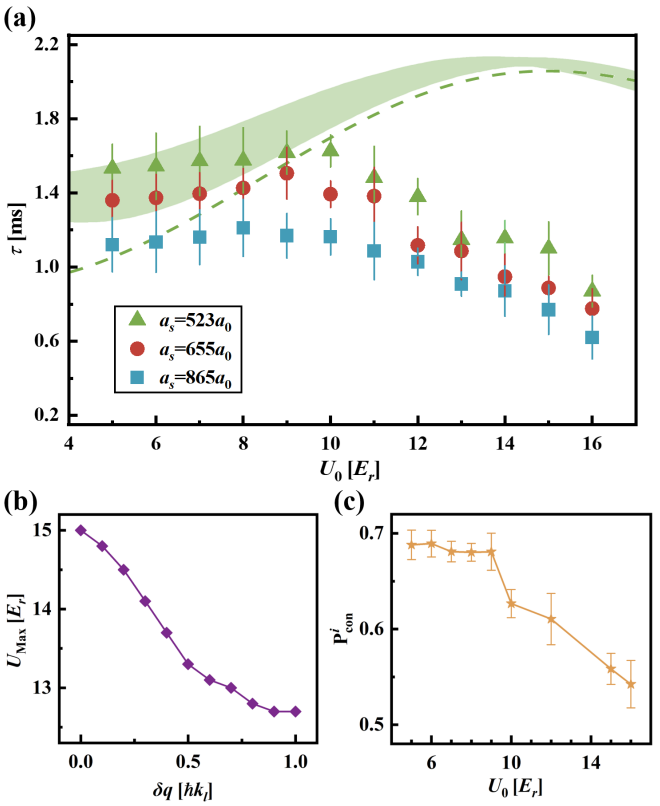

FIG. 4. (a) The D-band lifetimes with varying U_0 ($n_D = 1.0\times10^{18}$ m^{-3}) are shown under different values of a_s. The green triangles, red circles, and blue squares represent the experimental results for $a_s = 523a_0$, $655a_0$, and $865a_0$, respectively. The theoretical results with momentum broadening, $\delta q = 0$, and $0.1 \leqslant \delta q/\hbar k_l \leqslant 0.5$ are depicted by the green dashed line and the green shading, respectively. (b) The theoretical peak lattice depth U_{Max} as a function of momentum width δq. (c) The condensed fraction P^i_{con} on completion of band preparation ($t_{\mathrm{evo}} = 0$), for various lattice depths.

B. Variation of the D-band lifetime with lattice depth under different interactions

In our previous work [38], we predicted the existence of an optimal lattice depth for weakly interacting D-band bosons in various optical lattice configurations, including 1D lattices. However, its validity under stronger interaction regimes remains unclear. To explore this, we conduct experiments with varying U_0 at $a_s = 523a_0$, $655a_0$, and $865a_0$, as shown in Fig. 4(a). The experimental results suggest that, for $U_0 \leqslant 10E_r$, the D-band lifetime remains largely unchanged with a slight increase, whereas for $U_0 > 10E_r$, it decreases monotonically. The lifetime is maximized at around $10E_r$ without an explicit peak. It suggests other interaction effects on the excited-band lifetime, leading to the absence of a universal optimal lattice depth for the D band within the strongly interacting regime.

By performing numerical calculations, we obtain the lifetimes for different lattice depths U_0 at $a_s = 523a_0$ [green dashed line in Fig. 4(a)]. The D-band lifetime initially increases, reaching a maximum and then decreases as U_0 continues to rise. This behavior can be explained by the nonmonotonic variation of the overlap integral in Eq. (2) [38]. As U_0 increases, the two-body D-band Bloch wave function, $u^2_{D,0}(x)$, first localizes at the central peak, then spreads out to the two side peaks, and eventually relocalizes at the center. As a result, the theoretical D-band lifetime changes with the sum of scattering cross sections shown in Fig. 1(b), exhibiting this trend. Although both the theoretical predictions and experimental results exhibit a similar trend, featuring a peak and subsequent decline, a significant discrepancy exists between them. From a qualitative perspective, the discrepancy may be attributed to several primary factors.

The first factor is the non-negligible momentum broadening arising from the strong interaction strength, especially when $a_s > 500a_0$. As shown in Fig. 2(c), the quasimomentum broadening width of the condensate is substantial and increases with increasing scattering length. In this situation, the momentum distribution in the vicinity of the Γ point can no longer be approximated as a δ function. We instead approximate the two-body quasimomentum distribution as a Gaussian function:

$$\Xi(q_1, q_2) = \frac{1}{2\pi\delta q^2} e^{-\frac{q_1^2+q_2^2}{2\delta q^2}}, \tag{7}$$

where q_i is the quasimomentum of the two particles and δq is the quasimomentum broadening width in the D band. Using Eqs. (3) and (4), we calculate the D-band lifetime as a function of lattice depth for different values of δq. The theoretical lifetime interval for $0.1 \leqslant \delta q/\hbar k_l \leqslant 0.5$ at $a_s = 523a_0$, with the initial D-band density $n_D^i = 1.0\times10^{18}$ m^{-3} (approximated by the mBEC density), is shown in Fig. 4(a) with the green shading. As δq increases, τ increases in the shallow lattice, while the magnitude of its variation decreases, and its maximum shifts to a lower U_0, as illustrated in Fig. 4(b), which qualitatively agree better with our experimental results compared to the nonbroadening case. While this adjustment does not achieve perfect agreement between experimental and theoretical results, it does bring them closer in terms of the observed trend. Therefore, we consider this to be a potentially contributing factor. It is important to note that δq cannot be easily deduced from our experiment because the D-band particles separate into two clusters after band mapping, and the TOF process is affected by interaction effects. Thus the actual momentum broadening is smaller than that directly inferred from measurements in quasimomentum space ($\sim 0.4\hbar k$).

The second factor is the decoherence during both the preparation and evolution stages. As shown in Fig. 4(c), the initial condensed fraction P^i_{con} (the fraction of particles in the D-band condensates) after the band preparation ($t_{\text{evo}} = 0$) exhibits a significant decrease around $U_0 = 10E_r$, indicating a substantial reduction in coherence for $U_0 > 10E_r$. The increased presence of noncondensed particles amplifies the collisions between those and coherent particles, resulting in elevated scattering rates. This may explain the rapid decrease in lifetime when $U_0 > 10E_r$. Furthermore, factors in the evolution stage, such as fluctuations, nonuniformity, and localization, may also reduce coherence and thereby impact lifetime. First, the lattice laser power increases with U_0, amplifying noise within the lattice system. This noise encompasses intensity fluctuations and thermal fluctuations. These are exacerbated by higher laser power and have been shown in interferometric systems to irreversibly degrade coherence [41]. Second, a deeper lattice enhances the harmonic confinement, leading to increased nonuniformity within the system and accelerating decoherence. Third, larger U_0 corresponds to reduced tunneling J, signifying enhanced localization and consequently contributes to increased decoherence within the system. These factors can accelerate the system's thermalization, converting some of the condensed particles into thermal ones, thus revealing faster scattering rates and consequently shorter lifetimes. Therefore, we consider this to be a potentially contributing factor. Further advances in experimental techniques are essential to obtain more conclusive empirical evidence of decoherence's impact on lifetime.

Beyond these two factors, several experimental factors could contribute to this discrepancy. These include the enhanced on-site interactions arising from the increased lattice depth, variations in on-site density due to lattice loading, and differing fidelities of the shortcut loading method across various lattice depths. Although isolating and measuring these effects individually presents experimental challenges, they warrant further investigation in future experiments.

In conclusion, these factors could all contribute to the increased lifetime in shallow lattices, the reduced lifetime in deep lattices and leftward shift of the peak observed. They may qualitatively account for the trend differences between the experimental results and theoretical predictions. However, further research is required to establish a robust theoretical foundation capable of providing a quantitative interpretation of these observations.

V. DISCUSSION ON THE COLLISIONAL SCATTERING PROCESS IN 1D OPTICAL LATTICES

A. Scattering process in a strongly interacting system

To distinguish the scattering channel of D-band molecules in a 1D optical lattice with remarkable interactions, we perform the D-band experiment with a molecular number density $n_d = 1.0\times10^{18}$ m^{-3} and a lattice depth of $U_0 = 10E_r$ to investigate the collisional scattering process in the D band. To minimize the scattering halo resulting from in-trap and time-of-flight collision, we choose the minimum scattering length $a_s = 523a_0$. The band-mapping distributions against t_{evo} are shown in Fig. 5(a1).

Despite the minimum scattering length used in our experiment, a scattering halo still covers the lower band distribution after band mapping. A typical TOF image is presented in Fig. 5(b1) with $t_{\text{evo}} = 2$ms. Aside from the D-band parts (the yellow solid line), we observe two additional condensates (the red dashed line) in the second BZ through the fitting. Note that particles in the P band possess a negative effective mass, causing them to gradually shift to $\pm\hbar k_l$ in the presence of an external harmonic trap. Thus, these condensates correspond to P-band particles. Since the scattered particles consist of both condensates and thermal clouds, we determine band fractions

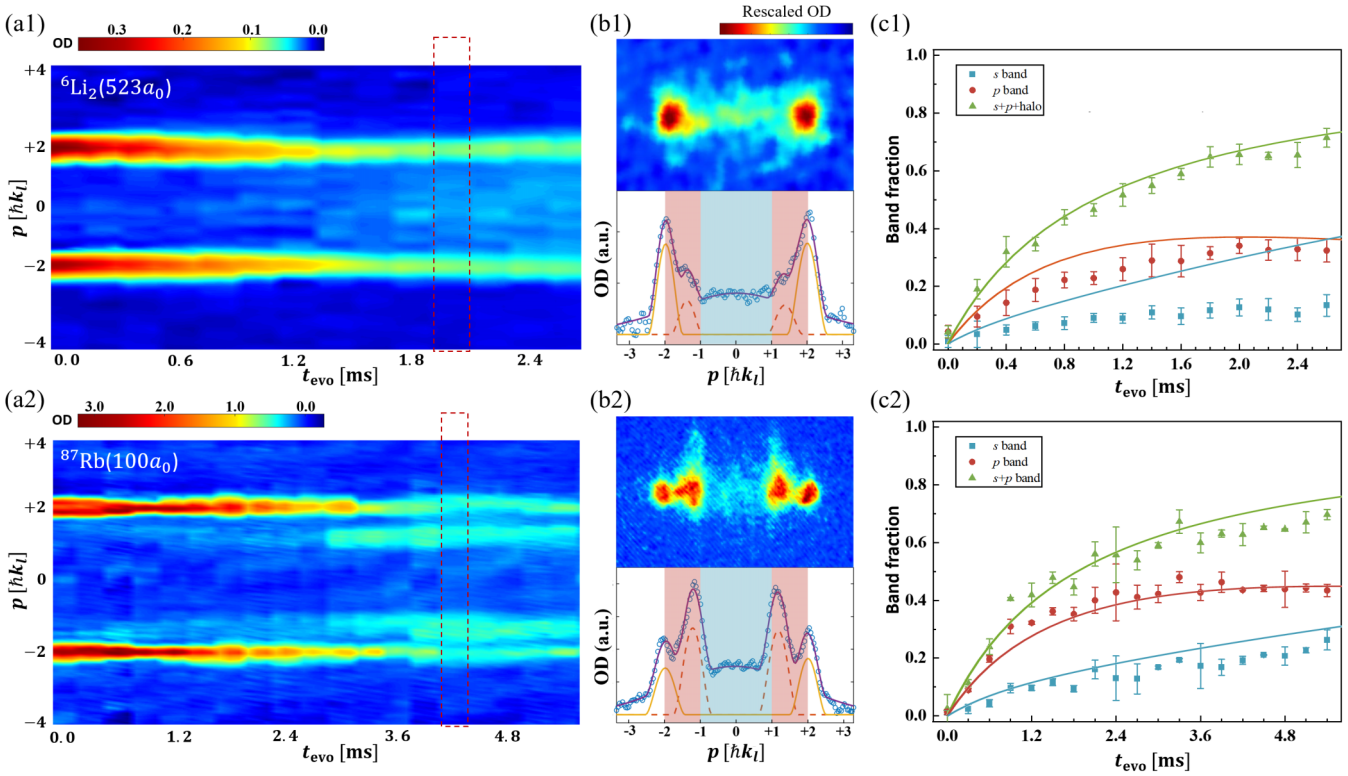

FIG. 5. (a) The collisional scattering process of D-band molecules under $U_0 = 10E_r$. Band-mapping distributions are plotted against evolution time $t_{\rm evo}$. (b) Top: Raw images of the red dashed boxes in (a) and (bottom) the corresponding 1D density distribution along the lattice. The first and second BZs are indicated by blue and red shading, respectively. The D-band condensed parts are shown by yellow solid lines. The P-band condensed parts are marked by red dashed lines. (c) The variation curves of the particle numbers in different bands. Blue squares and red circles represent the scattered particle numbers in the S and P bands, respectively. Green triangles represent all scattered particles except for those in the D band. The solid lines represent the solution of the rate equation accounting for the secondary scattering. [(a1), (b1), and (c1)] $^6Li_2$ molecules ($a_s = 523a_0$, $n_D = 1.0\times10^{18}$ m^{-3}, $t_{\rm map} = 0.1$ ms). [(a2), (b2), and (c2)] ^{87}Rb atoms ($a_s = 100a_0$, $n_D = 1.0\times10^{20}$ m^{-3}, $t_{\rm map} = 0.5$ ms).

by integrating the first term in Eq. (6) within the first BZ (S band, the blue shading) and second BZ (P band, the red shading) as well as the S-band parts (hardly any) and P-band parts (the red dashed line) in the second term, respectively. Moreover, the proportion of scattering halos at $t_{\rm evo} = 0$ ms is subtracted from the total particle number to eliminate disturbance from the scattering halos.

As shown in Fig. 5(c1), it is evident that the increase of particle number in the P band is significantly higher than in the S band, suggesting that the dominant scattering channel is $(D, D) \rightarrow (P, P)$. It exhibits a consistent conclusion with the prediction in Sec. II. However, interactions disrupt the information of scattered particles, and thus the conclusion regarding the substantial accumulation in the P band can only be inferred through fitting rather than observed directly.

B. Scattering process in a weakly interacting system

To observe scattering channels and the secondary scattering process more clearly, we repeat the experiment in a weakly interacting ^{87}Rb system ($a_s = 100a_0$) due to the difficulty of further reducing interactions in the $^6Li_2$ system. The experimental results, with the atomic number density $n_D = 1.0\times10^{20}$ m^{-3} and lattice depth $U_0 = 10E_r$, are shown in Fig. 5(a2). A more detailed description of this system is given in Ref. [42], and the scattering halo effect is mostly suppressed here. After an evolution time of $t_{\rm evo} = 1$ ms, a significant distribution of particles at $\pm\hbar k_l$ states is directly observed, as demonstrated by Fig. 5 for $t_{\rm evo} = 4.2$ ms. We present the obtained band fractions in Fig. 5(c2) and it also suggests that the $(D, D) \rightarrow (P, P)$ process is the relatively dominant scattering channel.

Additionally, we observe a slight decline of P-band distribution after 3 ms, which becomes more pronounced after 5.4 ms. It may be attributed to the enhancement of secondary scattering. To explain this, we develop a rate equation (see Appendix B for details) by considering all scattering channels from the D band and the secondary scattering from the P band to simulate the variation curves of band fractions in the S, P, and D bands. The solutions of the rate equation are represented by the solid lines in corresponding colors in Fig. 5(c2). The solutions fit well with the experimental data, especially of the proportion of P-band scattered particles. The contribution of the secondary scattering plays a significant role, preventing the P-band proportion from increasing monotonically (see Appendix B for results without the secondary scattering). They all suggest that the excited-band scattering theory is

quite robust in a weakly interacting system. Nonetheless, the theoretical model does not work well in our $^6Li_2$ system [solid lines in Fig. 5(c1)], which means it needs further modification to become more applicable for systems in the strongly interacting regime.

VI. CONCLUSION

In this work, we explore the effects of interactions on the collisional scattering of D-band $^6Li_2$ molecules in a 1D optical lattice with the shortcut loading method. By measuring the lifetimes of D-band particles under various interaction strengths, we experimentally investigate the squared relationship between the scattering rate of excited-band particles and the s-wave scattering length. It remains valid within a certain strongly interacting regime but breaks down as the scattering length diverges, supported by our experimental results. Meanwhile, interactions affect the trend of D-band lifetime varying with lattice depth, shifting the lifetime maximum to shallower depths compared to theoretical predictions and precluding the identification of an explicit optimal lattice depth. Possible contributing factors are discussed here to provide direction for future theoretical and experimental investigations.

Moreover, we analyze and discuss the scattering process of D-band particles. In the strongly interacting $^6Li_2$ system, we observe the dominant scattering channel $(D, D) \rightarrow (P, P)$ by fitting, but scattering halos induced by interactions hinder our direct detection of detailed scattering phenomena. For comparison, we conduct the same experiments in a weakly interacting ^{87}Rb system and observe more details. The rate equation developed in this study accurately calculates the evolution of band fractions when accounting for secondary scattering.

This work enhances our understanding of the interplay between interactions and collisional scattering of excited-band particles in optical lattices, paving the way for future research into many-body physics in lattice systems.

ACKNOWLEDGMENTS

This work is supported by the National Natural Science Foundation of China (Grants No. 92365208, No. 11934002, and No. 11920101004) and National Key Research and Development Program of China (Grants No. 2021YFA0718300 and No. 2021YFA1400900). C.L. is supported by the Austrian Science Fund (FWF) through the ESPRIT grant 'Entangled Atom Pair Quantum Processor' [Grant No. DOI: 10.55776/ESP310 (EAPQuP)]. The authors thank Chi Zhang for the discussion related to coding.

APPENDIX A: D-BAND SHORTCUT SEQUENCES

The shortcut method is a robust way to load BEC from the harmonic trap into optical lattices. In our previous work [14,35,49], we have used the method to load bosons into S band and excited bands of 1D, 2D, or 3D lattice. The basic principle of shortcut is that the evolution operators $L_{\vec{k}}(t)$ of momentum states $|\vec{k}\rangle$ are different between the lattice on and off. As shown in Fig. 2(c), after several laser pulses, the final state is

$$|\psi_f\rangle = \sum_{\vec{k}} \prod_{i=1}^{n} L_{\vec{k}}^{\text{off}}\left(t_i^{\text{off}}\right) L_{\vec{k}}^{\text{on}}\left(t_i^{\text{on}}\right) \times |\vec{k}\rangle, \tag{A1}$$

where n is the number of pulses and $L_{\vec{k}}^{\text{on/off}}(t)$ is the evolution operator when the lattice is on/off.

By choosing the number of pulses and pulse length, we can optimize the final state $|\psi_f\rangle$ to aimed state $|\psi_a\rangle$. The fidelity is defined by $|\langle\psi_f|\psi_a\rangle|^2$ to describe the loading efficiency. In the experiment, the optimized sequence has two pulses to load atoms into the D band of 1D optical lattices, and the pulse sequences of different lattice depths are shown in Table I. The theoretical fidelity is calculated under noninteraction conditions.

If interactions are considered, then the loading fidelity of the shortcut method decreases somewhat. As an example, the theoretical fidelity at $U_0 = 10E_r$ with strong interactions is calculated by the Gross-Pitaevskii equation and demonstrated in Table II. Although there is a drop, we cannot observe condensates in other bands experimentally. Thus we conclude that this method is still valid within the strongly interacting regime.

TABLE I. The shortcut sequences to load bosons into the D band in 1D optical lattices with different lattice depth.

V_0	t_1^{on} (μs)	t_1^{off}	t_2^{on}	t_2^{off}	Theoretical fidelity
$5E_r$	4.4	11.2	7.3	5.7	99.992%
$7E_r$	9.1	2.3	7.6	23.7	99.995%
$10E_r$	2.9	6.0	8.3	5.4	99.992%
$12E_r$	9.9	14.2	0.5	13.7	99.988%
$14E_r$	5.0	10.3	9.7	22.4	99.860%

APPENDIX B: RATE EQUATION OF THE EXCITED-BAND SCATTERING PROCESS

In this section, we develop a rate equation to evaluate the scattering process in the excited band. For the first scattering event, particles in the D band scatter into the S and P bands with different quasimomenta. We define the first scattering rate per unit density as follows:

$$\begin{aligned} R_{1,DP} &= \sigma(D, D; P, P)v + \tfrac{1}{2}\sigma(D, D; D, P)v, \\ R_{1,DS} &= \sigma(D, D; S, S)v, \end{aligned} \tag{B1}$$

where $\sigma(n_1, n_2; n_1', n_2')$ is defined in Eq. (3), and the channels $(D, D) \rightarrow (S, D)$, (S, P) are neglected here due to their minimal scattering cross sections. After the first scattering event, P-band particles can continue to scatter into the S band, a process we call secondary scattering. We now evaluate the

TABLE II. The D band fidelity of shortcut method in 1D optical lattices with different interaction strengths ($U_0 = 10E_r$).

a_s	$523a_0$	$655a_0$	$865a_0$	$1100a_0$	$1330a_0$	$1600a_0$
Fidelity	99.992%	99.992%	99.991%	99.991%	99.990%	99.988%

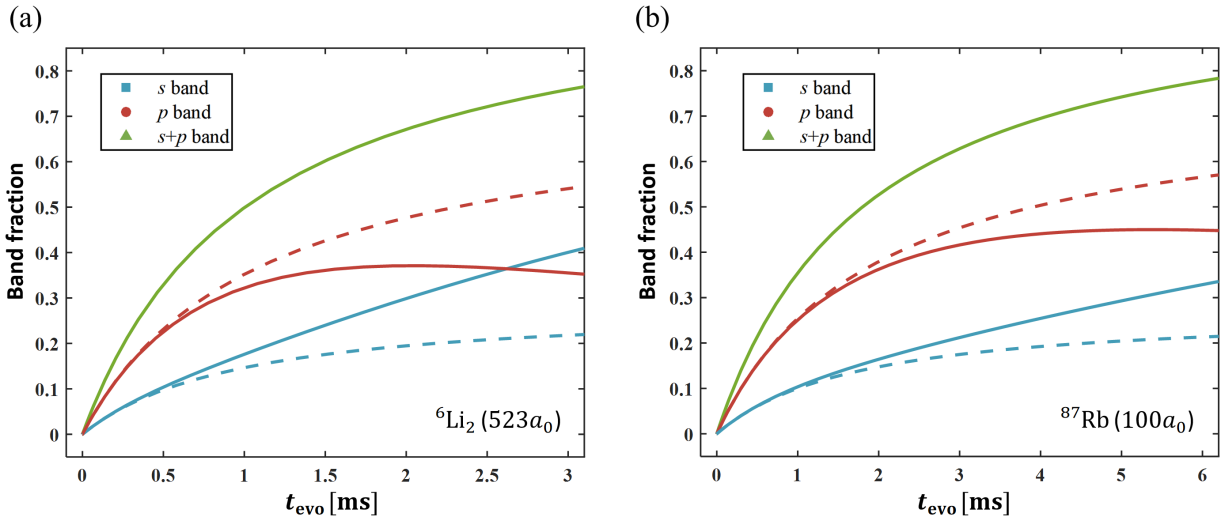

FIG. 6. The solution of rate equations in (a) $^6Li_2$ molecules system ($a_s = 523a_0$, $n_D = 1.0\times10^{18}$ m^{-3}) and (b) ^{87}Rb atoms system ($a_s = 100a_0$, $n_D = 1.0\times10^{20}$ m^{-3}). The red and green solid lines depict the fractional changes of the P and S bands, respectively, after incorporating secondary scattering. For comparison, the red and green dashed lines show the corresponding fractional changes in the P and S bands without considering secondary scattering. The difference between the solid and dashed lines thus quantifies the contribution of secondary scattering to the band fractions. The green solid line represents the change in the sum of the S-band and P-band fractions.

secondary scattering rate, $R_{2,PS} = \sigma(P,P;S,S)v$, from the P band at different q states to the S band. The P-band quasimomentum distribution, $f_P(q)$, after first scattering from the D band can be approximated by the overlap integral:

$$f_P(q) = \frac{\left|\Gamma^{D,D}_{P,P}(0,0;q,-q)\right|^2}{\int \mathrm{d}q\left|\Gamma^{D,D}_{P,P}(0,0;q,-q)\right|^2}, \tag{B2}$$

which is the normalized differential scattering cross section of the D band to the P band. Note that the $(D,D)\rightarrow(D,P)$ process is neglected in the secondary scattering process for simplicity. With this distribution, we set $\Xi(q_1,q_2) = f_P(q_1)f_P(q_2)$ in $\sigma(P,P;S,S)v$ and obtain $R_{2,PS}$. Combining both the first and secondary scattering processes, the differential equations governing the evolution of the scattering process are given by:

$$\begin{aligned}\frac{\mathrm{d}n_D}{\mathrm{d}t} &= -R_{1,DP}n_D^2 - R_{1,DS}n_D^2,\\ \frac{\mathrm{d}n_P}{\mathrm{d}t} &= R_{1,DP}n_D^2 - R_{2,PS}n_P^2,\\ \frac{\mathrm{d}n_S}{\mathrm{d}t} &= R_{1,DS}n_D^2 + R_{2,PS}n_P^2,\end{aligned} \tag{B3}$$

with the initial condition: $n_D(0) = n_D^i$, $n_S(0) = n_P(0) = 0$. The solution of these equations, with and without $R_{2,PS}$, is displayed in Fig. 6. The experimental data in Fig. 5 suggest that secondary scattering plays a significant role in practice.

[1] I. Bloch, J. Dalibard, and W. Zwerger, Many-body physics with ultracold gases, Rev. Mod. Phys. **80**, 885 (2008).

[2] M. Greiner, O. Mandel, T. Esslinger, T. W. Hänsch, and I. Bloch, Quantum phase transition from a superfluid to a Mott insulator in a gas of ultracold atoms, Nature (London) **415**, 39 (2002).

[3] R. Jördens, N. Strohmaier, K. Günter, H. Moritz, and T. Esslinger, A Mott insulator of fermionic atoms in an optical lattice, Nature (London) **455**, 204 (2008).

[4] J. Simon, W. S. Bakr, R. Ma, M. E. Tai, P. M. Preiss, and M. Greiner, Quantum simulation of antiferromagnetic spin chains in an optical lattice, Nature (London) **472**, 307 (2011).

[5] A. Mazurenko, C. S. Chiu, G. Ji, M. F. Parsons, M. Kanász-Nagy, R. Schmidt, F. Grusdt, E. Demler, D. Greif, and M. Greiner, A cold-atom Fermi–Hubbard antiferromagnet, Nature (London) **545**, 462 (2017).

[6] J. Struck, C. Ölschläger, R. L. Targat, P. Soltan-Panahi, A. Eckardt, M. Lewenstein, P. Windpassinger, and K. Sengstock, Quantum simulation of frustrated classical magnetism in triangular optical lattices, Science **333**, 996 (2011).

[7] D. Greif, T. Uehlinger, G. Jotzu, L. Tarruell, and T. Esslinger, Short-range quantum magnetism of ultracold fermions in an optical lattice, Science **340**, 1307 (2013).

[8] U. Schneider, L. Hackermüller, S. Will, T. Best, I. Bloch, T. A. Costi, R. W. Helmes, D. Rasch, and A. Rosch, Metallic and insulating phases of repulsively interacting fermions in a 3D optical lattice, Science **322**, 1520 (2008).

[9] M. Schreiber, S. S. Hodgman, P. Bordia, H. P. Lüschen, M. H. Fischer, R. Vosk, E. Altman, U. Schneider, and I. Bloch, Observation of many-body localization of interacting fermions in a quasirandom optical lattice, Science **349**, 842 (2015).

[10] M. E. Tai, A. Lukin, M. Rispoli, R. Schittko, T. Menke, D. Borgnia, P. M. Preiss, F. Grusdt, A. M. Kaufman, and M. Greiner, Microscopy of the interacting Harper-Hofstadter model in the two-body limit, Nature (London) **546**, 519 (2017).

[11] G. Jotzu, M. Messer, R. Desbuquois, M. Lebrat, T. Uehlinger, D. Greif, and T. Esslinger, Experimental realization of the topological Haldane model with ultracold fermions, Nature (London) **515**, 237 (2014).

[12] X. Li, A. Paramekanti, A. Hemmerich, and W. V. Liu, Proposed formation and dynamical signature of a chiral Bose liquid in an optical lattice, Nat. Commun. **5**, 3205 (2014).

[13] T. Müller, S. Fölling, A. Widera, and I. Bloch, State preparation and dynamics of ultracold atoms in higher lattice orbitals, Phys. Rev. Lett. **99**, 200405 (2007).

[14] L. Niu, S. Jin, X. Chen, X. Li, and X. Zhou, Observation of a dynamical sliding phase superfluid with *P*-band bosons, Phys. Rev. Lett. **121**, 265301 (2018).

[15] S. Jin, W. Zhang, X. Guo, X. Chen, X. Zhou, and X. Li, Evidence of Potts-nematic superfluidity in a hexagonal sp^2 optical lattice, Phys. Rev. Lett. **126**, 035301 (2021).

[16] X.-Q. Wang, G.-Q. Luo, J.-Y. Liu, W. V. Liu, A. Hemmerich, and Z.-F. Xu, Evidence for an atomic chiral superfluid with topological excitations, Nature (London) **596**, 227 (2021).

[17] Y. Kiefer, M. Hachmann, and A. Hemmerich, Ultracold Feshbach molecules in an orbital optical lattice, Nat. Phys. **19**, 794 (2023).

[18] C. J. Fujiwara, K. Singh, Z. A. Geiger, R. Senaratne, S. V. Rajagopal, M. Lipatov, and D. M. Weld, Transport in Floquet-Bloch bands, Phys. Rev. Lett. **122**, 010402 (2019).

[19] Z. Yu, J. Tian, P. Peng, D. Mao, X. Chen, and X. Zhou, Transport of ultracold atoms in superpositions of *S*- and *D*-band states in a moving optical lattice, Phys. Rev. A **107**, 023303 (2023).

[20] F. Kemper, F. Rosicky, and R. Feder, Relativistic two-channel theory of elastic electron-atom scattering and application to He and Ne, J. Phys. B: At. Mol. Opt. Phys. **17**, 3763 (1984).

[21] M. Olshanii, Atomic scattering in the presence of an external confinement and a gas of impenetrable bosons, Phys. Rev. Lett. **81**, 938 (1998).

[22] J. Weiner, V. S. Bagnato, S. Zilio, and P. S. Julienne, Experiments and theory in cold and ultracold collisions, Rev. Mod. Phys. **71**, 1 (1999).

[23] T. Bergeman, M. G. Moore, and M. Olshanii, Atom-atom scattering under cylindrical harmonic confinement: Numerical and analytic studies of the confinement induced resonance, Phys. Rev. Lett. **91**, 163201 (2003).

[24] J. M. Hutson, M. Beyene, and M. L. González-Martínez, Dramatic reductions in inelastic cross sections for ultracold collisions near Feshbach resonances, Phys. Rev. Lett. **103**, 163201 (2009).

[25] H. Konishi, F. Schäfer, S. Ueda, and Y. Takahashi, Collisional stability of localized Yb($^3P_2$) atoms immersed in a Fermi sea of Li, New J. Phys. **18**, 103009 (2016).

[26] F. H. J. Hall and S. Willitsch, Millikelvin reactive collisions between sympathetically cooled molecular ions and laser-cooled atoms in an ion-atom hybrid trap, Phys. Rev. Lett. **109**, 233202 (2012).

[27] R. Saito, S. Haze, M. Sasakawa, R. Nakai, M. Raoult, H. Da Silva, O. Dulieu, and T. Mukaiyama, Characterization of charge-exchange collisions between ultracold ^{6}Li atoms and $^{40}Ca^+$ ions, Phys. Rev. A **95**, 032709 (2017).

[28] D. Seitov, K. Nekrasov, A. Y. Kupryazhkin, S. Gupta, and A. Usseinov, The impact of the collision cascades on the xenon and helium clusters in PuO_2 crystals. a molecular dynamics simulation, Nucl. Instrum. Methods B **476**, 26 (2020).

[29] Y. Yu, G. S. Jung, C. Liu, Y. C. Lin, C. M. Rouleau, M. Yoon, G. Eres, G. Duscher, K. Xiao, S. Irle, A. A. Puretzky, and D. B. Geohegan, Strain-induced growth of twisted bilayers during the coalescence of monolayer MoS_2 crystals, ACS Nano **15**, 4504 (2021).

[30] R. Tyrrell, B. De Souza, and P. J. Frawley, Particle breakage: Limiting conditions for crystal-crystallizer collisions, Cryst. Growth Des. **18**, 617 (2018).

[31] A. Isacsson and S. M. Girvin, Multiflavor bosonic Hubbard models in the first excited bloch band of an optical lattice, Phys. Rev. A **72**, 053604 (2005).

[32] X. Li and W. V. Liu, Physics of higher orbital bands in optical lattices: A review, Rep. Prog. Phys. **79**, 116401 (2016).

[33] S. Paul and E. Tiesinga, Formation and decay of Bose-Einstein condensates in an excited band of a double-well optical lattice, Phys. Rev. A **88**, 033615 (2013).

[34] G. Lamporesi, J. Catani, G. Barontini, Y. Nishida, M. Inguscio, and F. Minardi, Scattering in mixed dimensions with ultracold gases, Phys. Rev. Lett. **104**, 153202 (2010).

[35] Y. Zhai, X. Yue, Y. Wu, X. Chen, P. Zhang, and X. Zhou, Effective preparation and collisional decay of atomic condensates in excited bands of an optical lattice, Phys. Rev. A **87**, 063638 (2013).

[36] F. Pinheiro, G. M. Bruun, J.-P. Martikainen, and J. Larson, *XYZ* quantum Heisenberg models with *p*-orbital bosons, Phys. Rev. Lett. **111**, 205302 (2013).

[37] X. Guo, Z. Yu, P. Peng, G. Yin, S. Jin, X. Chen, and X. Zhou, Dominant scattering channel induced by two-body collision of *D*-band atoms in a triangular optical lattice, Phys. Rev. A **104**, 033326 (2021).

[38] H. Shui, C.-K. Lai, Z. Yu, J. Tian, C. Wu, X. Chen, and X. Zhou, Optimal lattice depth on lifetime of D-band ultracold atoms in a triangular optical lattice, Opt. Express **31**, 26599 (2023).

[39] G. Chatelain, N. Dupont, M. Arnal, V. Brunaud, J. Billy, B. Peaudecerf, P. Schlagheck, and D. Guéry-Odelin, Observation and control of quantized scattering halos, New J. Phys. **22**, 123032 (2020).

[40] N. Q. Burdick, A. G. Sykes, Y. Tang, and B. L. Lev, Anisotropic collisions of dipolar Bose-Einstein condensates in the universal regime, New J. Phys. **18**, 113004 (2016).

[41] D. Hu, L. Niu, S. Jin, X. Chen, G. Dong, J. Schmiedmayer, and X. Zhou, Ramsey interferometry with trapped motional quantum states, Commun. Phys. **1**, 29 (2018).

[42] H. Shui, S. Jin, Z. Li, F. Wei, X. Chen, X. Li, and X. Zhou, Atom-orbital qubit under nonadiabatic holonomic quantum control, Phys. Rev. A **104**, L060601 (2021).

[43] F. Wei, Z. Zhang, Y. Chen, H. Shui, Y. Liang, C. Li, and X. Zhou, Temporal Talbot interferometer of a strongly interacting molecular Bose-Einstein condensate, Phys. Rev. A **109**, 043313 (2024).

[44] C. Li, Q. Liang, P. Paranjape, R. G. Wu, and J. Schmiedmayer, Matter-wave interferometers with trapped strongly interacting Feshbach molecules, Phys. Rev. Res. **6**, 023217 (2024).

[45] S. Jochim, M. Bartenstein, A. Altmeyer, G. Hendl, S. Riedl, C. Chin, J. H. Denschlag, and R. Grimm, Bose-Einstein condensation of molecules, Science **302**, 2101 (2003).

[46] M. Bartenstein, A. Altmeyer, S. Riedl, R. Geursen, S. Jochim, C. Chin, J. H. Denschlag, R. Grimm, A. Simoni, E. Tiesinga,

C. J. Williams, and P. S. Julienne, Precise determination of ^{6}Li cold collision parameters by radio-frequency spectroscopy on weakly bound molecules, Phys. Rev. Lett. **94**, 103201 (2005).

[47] D. S. Petrov, C. Salomon, and G. V. Shlyapnikov, Weakly bound dimers of fermionic atoms, Phys. Rev. Lett. **93**, 090404 (2004).

[48] P. L. Kapitza and P. A. M. Dirac, The reflection of electrons from standing light waves, Math. Proc. Cambr. Philos. Soc. **29**, 297 (1933).

[49] X. Zhou, S. Jin, and J. Schmiedmayer, Shortcut loading a Bose-Einstein condensate into an optical lattice, New J. Phys. **20**, 055005 (2018).

[50] M. Greiner, I. Bloch, O. Mandel, T. W. Hänsch, and T. Esslinger, Exploring phase coherence in a 2D lattice of Bose-Einstein condensates, Phys. Rev. Lett. **87**, 160405 (2001).

[51] Y. Chen, Z. Zhang, C.-K. Lai, Y. Liang, H. Shui, H. Fu, F. Wei, and X. Zhou, Scattering halos in strongly interacting Feshbach molecular Bose-Einstein condensates, Phys. Rev. A **111**, 043303 (2025).